



Lawrence Berkeley Laboratory

UNIVERSITY OF CALIFORNIA

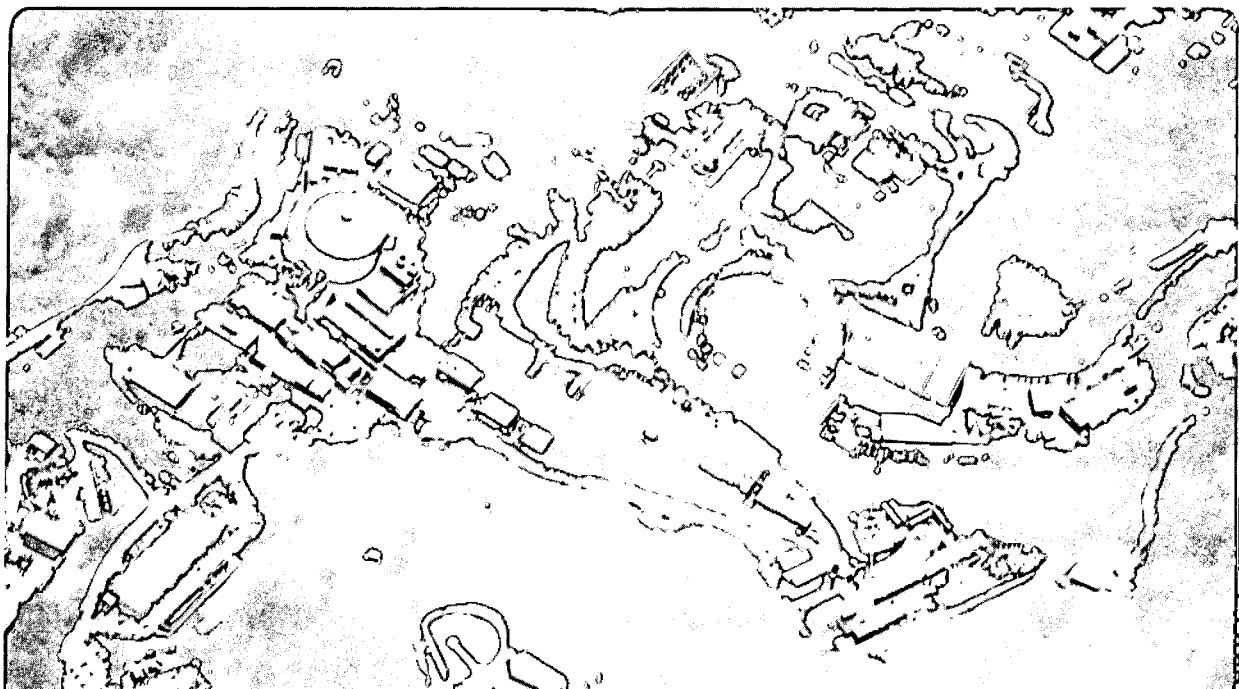
Physics Division

Invited paper presented at the Division of Particles and Fields (DPF92), Batavia, IL, November 10-14, 1992, and to be published in the Proceedings

Highlights from DØ

R.J. Madaras

December 1992



REFERENCE COPY
Does Not
Circulate

Copy 1

LBL-33320

DISCLAIMER

This document was prepared as an account of work sponsored by the United States Government. While this document is believed to contain correct information, neither the United States Government nor any agency thereof, nor the Regents of the University of California, nor any of their employees, makes any warranty, express or implied, or assumes any legal responsibility for the accuracy, completeness, or usefulness of any information, apparatus, product, or process disclosed, or represents that its use would not infringe privately owned rights. Reference herein to any specific commercial product, process, or service by its trade name, trademark, manufacturer, or otherwise, does not necessarily constitute or imply its endorsement, recommendation, or favoring by the United States Government or any agency thereof, or the Regents of the University of California. The views and opinions of authors expressed herein do not necessarily state or reflect those of the United States Government or any agency thereof or the Regents of the University of California.

HIGHLIGHTS FROM DØ

RONALD J. MADARAS

Physics Division
Lawrence Berkeley Laboratory*
University of California
Berkeley, California 94720

for the DØ Collaboration

DECEMBER 1992

*This work was supported by the Director, Office of Energy Research, Office of High Energy and Nuclear Physics, High Energy Physics Division, of the U.S. Department of Energy under Contract No. DE-AC03-76SF00098.

HIGHLIGHTS FROM DØ ¹

RONALD J. MADARAS

*Lawrence Berkeley Laboratory, University of California
Berkeley, CA 94720, USA*

for the DØ Collaboration

ABSTRACT

The DØ Experiment is a new, large multipurpose experiment at the Tevatron Proton-Antiproton Collider at the Fermi National Accelerator Laboratory. From the analysis of data taken during August–October, 1992, a selection of preliminary physics results will be given on inclusive jet production, direct photon production, the production and decay properties of the W and Z bosons, the search for the top quark in the dilepton and lepton + jets channels, B physics and searches for new particles.

1. The DØ Detector

The primary goal of the DØ Experiment^{1,2} is the precision study of high mass, large transverse momentum phenomena with particular emphasis on measurements of leptons (electrons and muons), photons, jets (clusters of produced particles), and missing transverse momentum indicative of penetrating particles (such as neutrinos). To accomplish this goal, the detector design stresses uniform, hermetic, fine-grained calorimetry, large solid angle coverage and excellent muon detection. The Detector is shown in Fig. 1. It includes three major components: the outer Muon System, the inner Central Tracking System, and the liquid argon Calorimeter System.

1.1. Muon System

The Muon System³ consists of five iron toroids, 1.1–1.5 meters thick, and three layers of proportional drift tube (PDT) chambers. The central toroid surrounds the calorimeter and covers angles down to 45°. The end toroids and the small angle muon system cover the forward region down to 5°. Thus there is full muon coverage for $|\eta| \leq 3.2$. The momentum of a muon is determined by using the PDT chambers to measure the deflection of the muon trajectory in the 1.9 T steel toroids. The momentum resolution, typically 20%, is dominated by multiple scattering for momenta < 80 GeV/ c . The combined calorimeter plus toroid thickness

¹Presented at the 7th Meeting of the American Physical Society Division of Particles and Fields (DPF92), November 10–14, 1992, Fermi National Accelerator Laboratory, Batavia, Illinois.

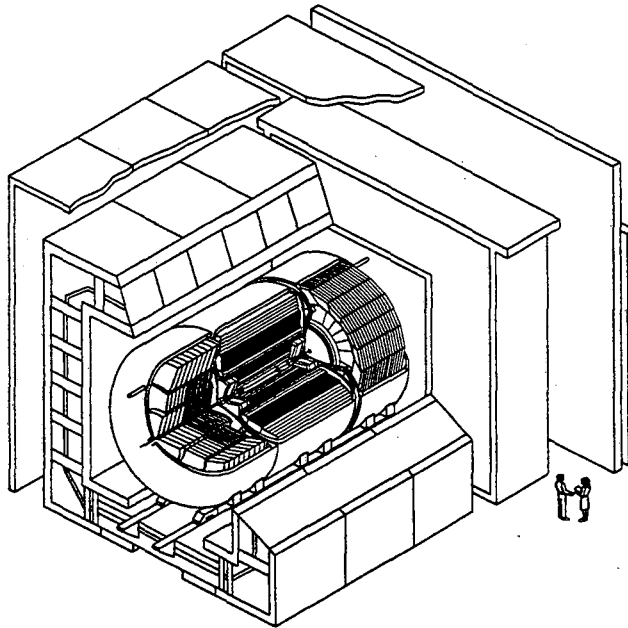


Figure 1: The DØ Detector

varies from 14λ in the central region to 19λ in the end regions. This thickness reduces backgrounds from hadronic punchthroughs to a negligible level.⁴

1.2. Central Tracking System

The Central Tracking System,⁵ shown in Fig. 2, consists of four main components: Vertex Chamber, Transition Radiation Detector, Central Drift Chamber and two sets of Forward Drift Chambers.

The Vertex Chamber⁶ has three cylindrical layers of jet-type cells, and every cell in a layer has eight sense wires. It provides precision charged particle tracking with good azimuthal spatial resolution ($60 \mu\text{m}$) and good two-track resolution (0.6 mm). Charge division is used to measure the axial coordinate with a resolution of about 1 cm . The chamber is also used to find secondary vertices, and reject photon conversions which can give a fake electron signal.

The Transition Radiation Detector⁷ provides additional rejection of pions in the identification of central electrons. It has three cylindrical layers, each layer consisting of a set of polypropylene foils surrounded by a radial drift X-ray detector. A pion rejection factor of 50 was achieved in a test beam for an electron efficiency of 90%.

The Central Drift Chamber⁸ has four cylindrical layers of jet-type cells, and every cell in a layer has seven sense wires. Its azimuthal spatial resolution is $150 \mu\text{m}$. The axial position of tracks is measured with delay lines, with a resolution of 4 mm . Measurements of dE/dx are used to help identify conversions.

The Forward Drift Chambers⁹ cover angles down to 5° , and include two

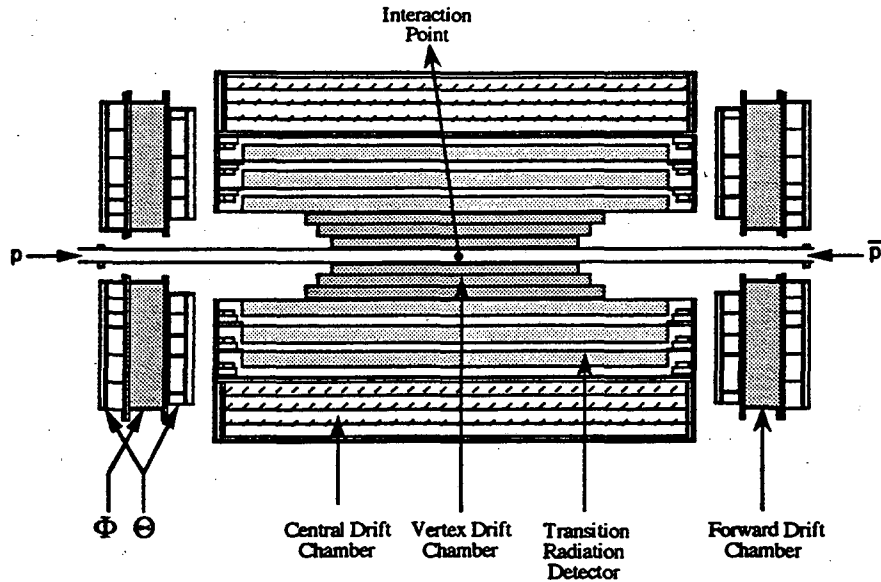


Figure 2: The DØ Central Tracking System.

types of units. The Φ units have radial sense wires, with 16 measurements along each track. The Θ units have sense wires oriented transversely to the beam, with 8 measurements along each track in each of the two units. The spatial resolution in each unit is $200 \mu\text{m}$.

1.3. Calorimeter System

The DØ calorimeters are sampling calorimeters using uranium as the absorbing material and liquid argon as the sampling medium. The use of uranium not only leads to a compact calorimeter design, but it helps in equalizing the calorimeter response to electrons and hadrons. This is important for minimizing the fluctuations in the observed energies of jets, whose particle content may vary. Liquid argon is used as the active ionization medium because of its ease of calibration, its stability and uniformity of response, and its radiation hardness.

The DØ Calorimeter System,^{10,11} shown in Fig. 3, consists of a cylindrical Central Calorimeter and two End Calorimeters covering angles down to within 1° of the beamline. Each of the three calorimeters contains an electromagnetic section with thin uranium plates, a fine hadronic section with thick uranium plates, and a coarse hadronic section with very thick copper or steel plates. Printed circuit boards with segmented detection pads are interleaved between the absorber plates to detect the ionization in the liquid argon. All of the DØ calorimeter modules use a uniform technology to facilitate the relative calibration between modules. The calorimeters are designed with minimal cracks and other uninstrumented regions in order to provide essentially hermetic coverage.

DØ LIQUID ARGON CALORIMETER

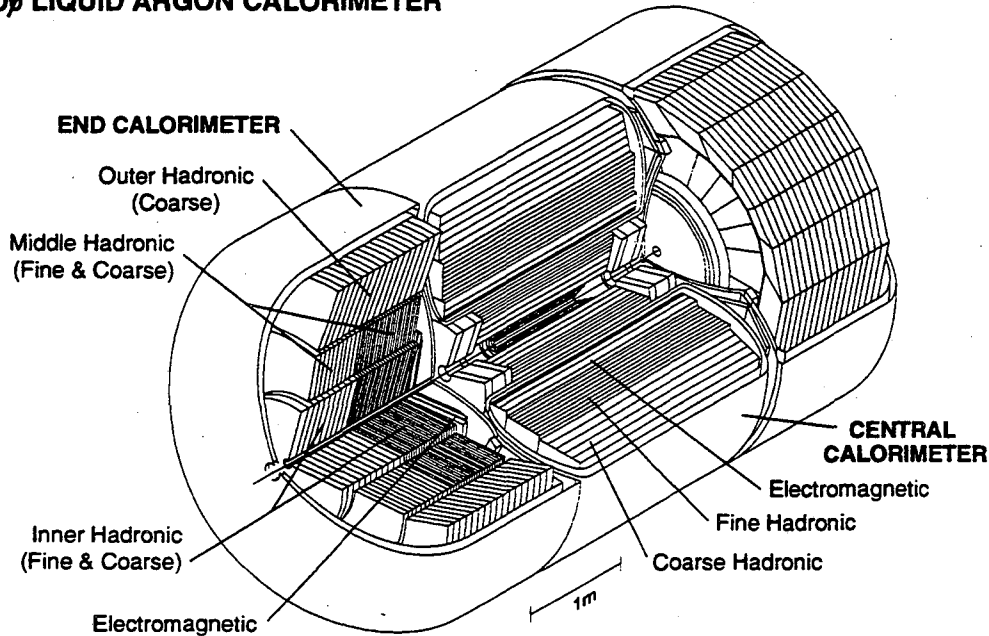


Figure 3: The DØ Calorimeter System.

The calorimeters are finely segmented both longitudinally and transversely. Longitudinally, each electromagnetic section is divided into 4 readout depths (for a total of $21 X_0$), and the hadronic sections are divided into 4–5 depths (for a total of 7–9 λ). The transverse segmentation is 0.1×0.1 for $\Delta\eta \times \Delta\phi$, except in the third electromagnetic longitudinal section (where shower maximum occurs), where the segmentation is increased to 0.05×0.05 for better shower position resolution. The readout cells are arranged in semi-projective towers.

Typical electromagnetic and hadronic calorimeter modules have been extensively tested with electrons and pions from 2 to 150 GeV in a test beam at FNAL.^{10,12,13} The fractional energy resolution of electrons in the calorimeters is $15\%/\sqrt{E}$, and of pions is $50\%/\sqrt{E}$. The spatial position resolution for electrons is 1–2 mm, for energies above 50 GeV. Using the transverse and longitudinal shower shape information from the electromagnetic and hadronic modules, a pion rejection factor of greater than 1000 has been measured for a 95% electron efficiency. The e/π response of the calorimeter system is energy dependent but varies within the range 1.04–1.12 for energies between 10 and 100 GeV.

The missing transverse energy \cancel{E}_T resolution of the DØ Calorimeter System, important for new particle searches and the precision measurement of the mass of the W boson, is excellent because of the calorimeter's hermeticity and uniformity. Figure 4a shows the distribution of the signed z component of the \cancel{E}_T for minimum bias collider data, for a total scalar transverse energy interval of 60–70 GeV. The distribution is well fit with a Gaussian, with a resolution of 2.3 GeV. The standard deviation of the z component of the \cancel{E}_T is plotted as a function of total scalar E_T

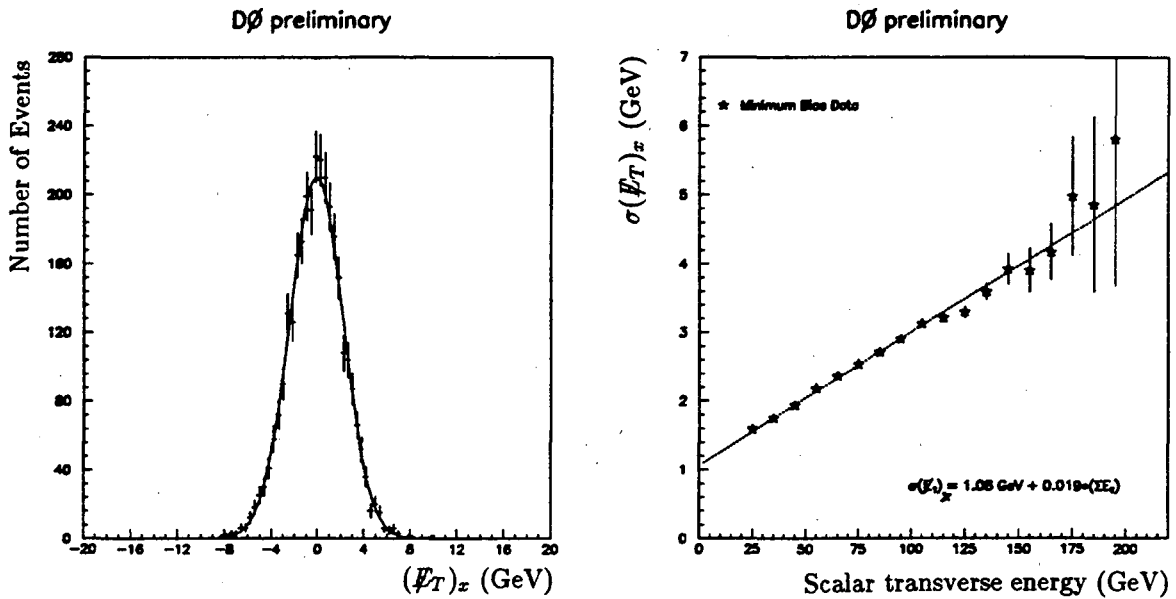


Figure 4: a) Signed x component of E_T for minimum bias collider data, for $60 < \text{scalar transverse energy} < 70$ GeV. b) The standard deviation of the x component of the E_T as a function of scalar transverse energy. The line is a linear fit to the data.

in Fig. 4b. One sees that the E_T resolution is 2–4 GeV for scalar E_T in the range 50–150 GeV.

1.4. Trigger

The DØ Trigger System¹⁴ is outlined in Fig. 5. The initial (Level 0) trigger uses scintillation counters on both sides of the interaction point to determine if a beam-beam interaction occurred during a particular beam crossing. This rate depends on the luminosity, but is typically 100 kHz. The next (Level 1) trigger¹⁵ is a hardware trigger using information from the Muon System and Calorimeter. Part of the calorimeter signal is split off, and electromagnetic and hadronic energy is summed separately for $\Delta\eta \times \Delta\phi = 0.2 \times 0.2$ trigger towers. The Level 1 trigger can then make cuts on various combinations of counts of EM and jet towers above E_T thresholds, missing and total scalar E_T above thresholds, and the number of muons. The Level 1.5 trigger uses more detailed information from the muon chambers to make a P_T cut for muon triggers. The Level 1/1.5 rate at the present time is 70 Hz, which will be increased to 200 Hz in the near future.

The Level 2 trigger¹⁶ is a software filter running on a farm of VAX 4000/60 microprocessors. There the full event readout is used, and fully developed algorithms identify and measure electrons, photons, jets and muons, and calculate more accurately the event missing E_T and total scalar E_T . The filter then makes cuts on various combinations of these objects, with various thresholds. The events passing Level 2 are written to tape. The Level 2 event rate is currently 2 Hz, which will be

D0 Trigger

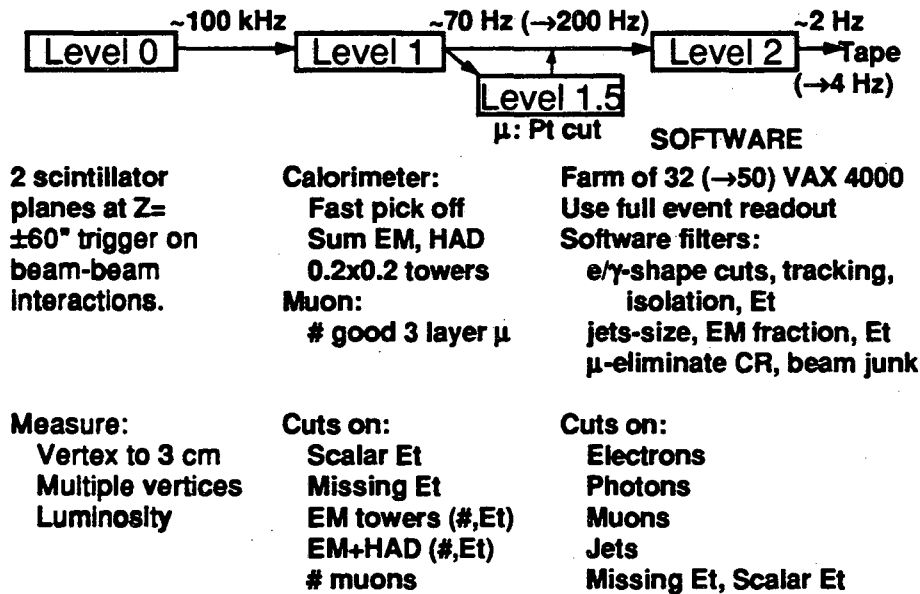


Figure 5: The D0 Trigger System.

increased to 4 Hz in the near future.

1.5 Operation at the Tevatron Collider

The D0 Detector saw its first $p\bar{p}$ collisions at the Fermilab Collider in May, 1992, when commissioning of the detector began with detailed studies of the trigger, backgrounds, and various detector elements. In August, 1992, we started our first physics data taking run with this detector. By the end of October, 1992, we had accumulated data on tape representing an integrated luminosity of 1.1 pb^{-1} . All of the results presented in the next section are based on data from that sample, and are preliminary.

2. Physics Analysis Highlights

2.1 Electroweak

Both $W \rightarrow \mu\nu$ and $Z \rightarrow \mu\mu$ have been detected in D0. Initial results¹⁷ for $W \rightarrow \mu\nu$ are given here for a luminosity of 410 nb^{-1} . The muons in this sample have $|\eta| < 1.0$, have a match to a central detector track, and have $P_T > 20 \text{ GeV}/c$. The missing P_T is $> 20 \text{ GeV}/c$ for the events. QCD background has been eliminated by requiring that the muon track be isolated in the calorimeter, and cosmic ray background has been reduced using drift timing from the muon chambers. Figure 6a shows the P_T spectrum for the muons, and Fig. 6b shows the W transverse mass for this sample of muons. In both cases, the Monte Carlo prediction (normalized to the luminosity) agrees with the data. The observed number of events is 25, including 6

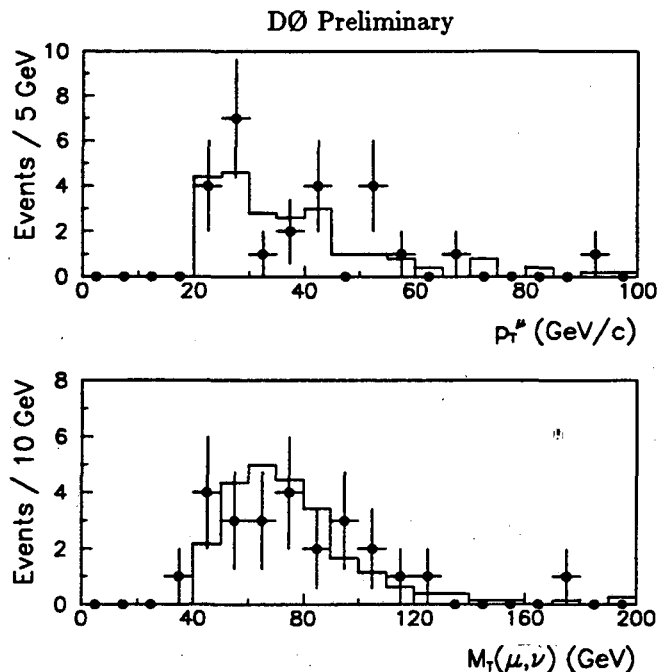


Figure 6: a) P_T spectrum for the muons in W boson events. b) W transverse mass for $W \rightarrow \mu\nu$ events. In both figures the points are data and the histogram is Monte Carlo.

background events, for a total of 19 W events. The expected number of W events, based on the luminosity, is 22 ± 5 events.

A clean $Z \rightarrow ee$ peak is seen in the data.¹⁸ Figure 7 shows the invariant mass distribution for di-electrons, in the 1.1 pb^{-1} data sample, with both electrons having $E_T > 20$ GeV. The electrons were identified as electromagnetic clusters having $< 10\%$ of their energy in the hadronic calorimeter sections, having a transverse and longitudinal cluster shape χ^2 which agrees with test beam expectations,¹⁹ and being isolated from the rest of the event. In addition, for one of the electrons a track was required to be found in the tracking chambers and to point to the calorimeter cluster. This tracking requirement was relaxed for the second electron. A Breit-Wigner fit to the 72 events, shown in Fig. 7, gives a peak at about 86 GeV. This is using the energy scale calibration directly from the test beam, without any corrections for the collider data, and is currently estimated to be correct to about 5%. Studies are underway to obtain a more precise energy scale.

A search¹⁸ for $W \rightarrow e\nu$ was made in the same 1.1 pb^{-1} sample that was used for the Z bosons. In addition to the cuts on the electron described in the preceding paragraph (including the tracking requirement), it was required that the event have $\cancel{E}_T > 20$ GeV. The resulting electron E_T spectrum is shown in Fig. 8. It falls off sharply at about 40 GeV, as expected for W events. The W transverse mass distribution for the 882 events is shown in Fig. 9, along with a fit to a curve whose shape is determined by Monte Carlo. It is seen that the expected shape, including the sharp Jacobian edge, agrees well with the distribution of the data points. One cannot extract a value for the W mass until the energy scale questions discussed

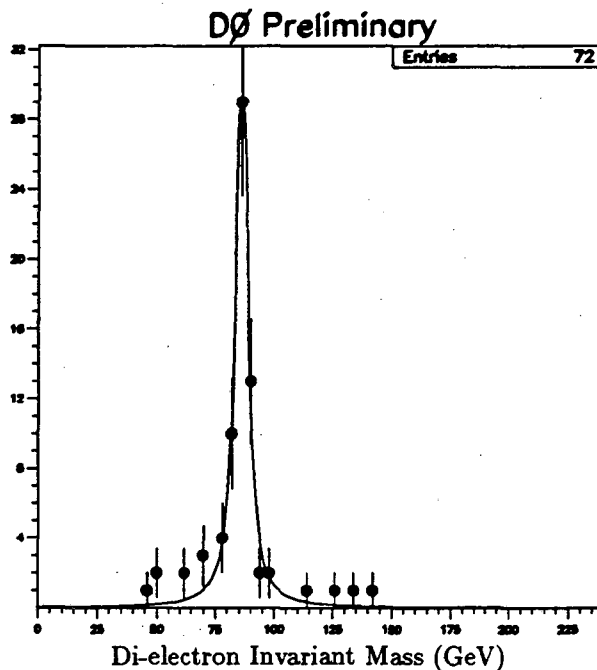


Figure 7: Di-electron invariant mass distribution, with a Breit-Wigner fit.

above are resolved. The cross section for W production times the branching ratio for $W \rightarrow e\nu$ is calculated from the above sample of events to be 2.3 ± 0.5 nb, in good agreement with published values.

2.2 Top

At the Tevatron Collider, top quark production and decay is expected to proceed via:

$$p\bar{p} \rightarrow t\bar{t} \rightarrow W^+W^-b\bar{b}$$

with the W bosons decaying into either lepton + neutrino, or jets. Thus in the final state one expects:

dileptons + jets + \cancel{E}_T , or

lepton + jets + \cancel{E}_T , or

all jets.

The search for top exploits the DØ detector's large angular acceptance for electrons, jets and muons, and its excellent missing E_T resolution.

A search for top was made in the di-electron channel.²⁰ Each electron was required to have a transverse and longitudinal shower shape χ^2 which agrees with test beam expectations,¹⁹ to be isolated from the rest of the event, and to have $E_T > 15$ GeV. Only one of the electrons was required to have a matching track. The dependence on azimuthal angle between electrons and the \cancel{E}_T for the resulting sample of 139 events is shown in Fig. 10. One sees a concentration of events from $Z \rightarrow ee$ in the upper left corner, and no events for $\Delta\phi(ee) < 160^\circ$ and $\cancel{E}_T > 20$ GeV. One would expect roughly 0.9 events in that region if the top quark mass were

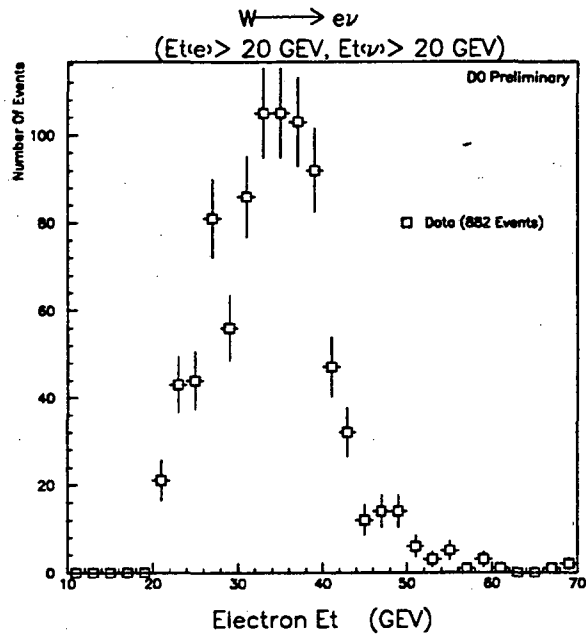


Figure 8: E_T spectrum for electrons in W boson events.

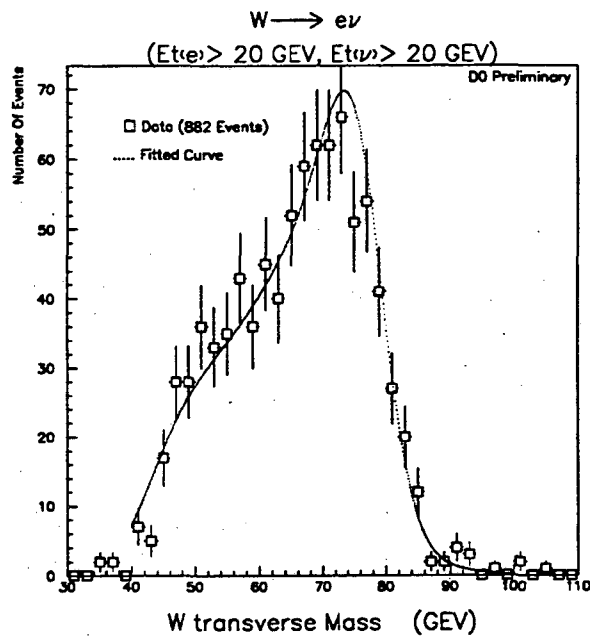


Figure 9: W transverse mass for $W \rightarrow e\nu$ events. The fit is discussed in the text.

DØ preliminary

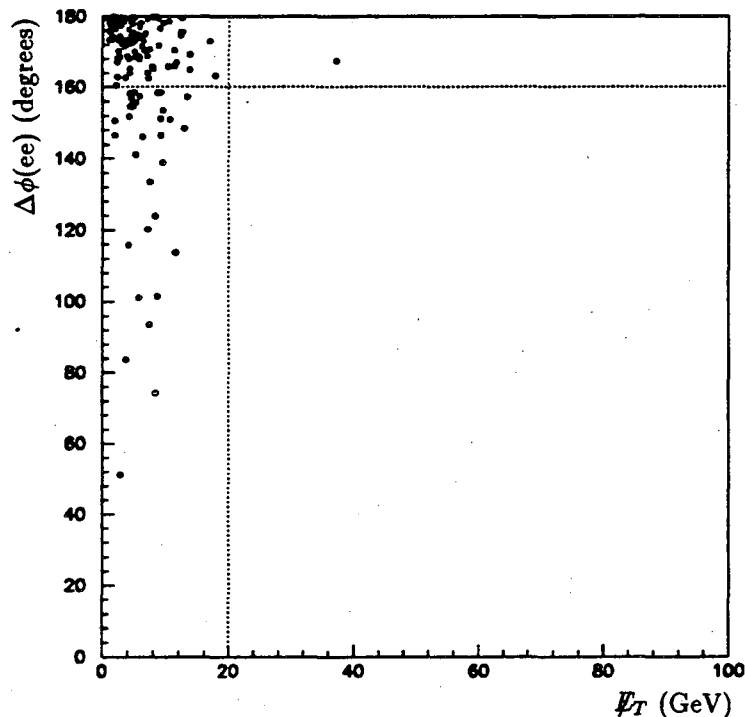


Figure 10: Azimuthal angle between di-electrons vs. \cancel{E}_T .

80 GeV.

A search was also made in the electron-muon channel.²⁰ Again the electron was required to have a shower shape χ^2 which agrees with test beam expectations,¹⁹ and to be isolated. But now $E_T > 8$ GeV, and the electron was not required to have a matching track. For the muons we required that $P_T > 8$ GeV, that the muon pointed back to the vertex, that there was a match between the muon track and the central tracking chambers, that there was no back-to-back track in the central tracker (to reject cosmic rays), and that the energy deposit in the calorimeter was appropriate for a muon. This resulted in a sample of six events. Figure 11 is a scatter plot for those events of the muon P_T and the electron E_T . It is seen that there are no events for $P_T(\mu) > 20$ GeV and $E_T(e) > 20$ GeV. One would expect roughly 0.6 events in that region if the top quark mass were 80 GeV.

Finally, a search was made in the electron+jets channel.²¹ The electron was required to pass the above shower shape and track matching cuts, and have $E_T > 20$ GeV. The number of jets with $E_T > 25$ GeV was required to be 3, and the $\cancel{E}_T > 20$ GeV. No events were left after these cuts. One would expect 2.6 ± 1.2 events after these cuts if the top quark mass were 80 GeV.

2.3 QCD

DØ, with its hermetic and finely segmented calorimeters, is ideal for a study of jet distributions. A particularly advantageous feature of DØ is its ability to

DØ Preliminary

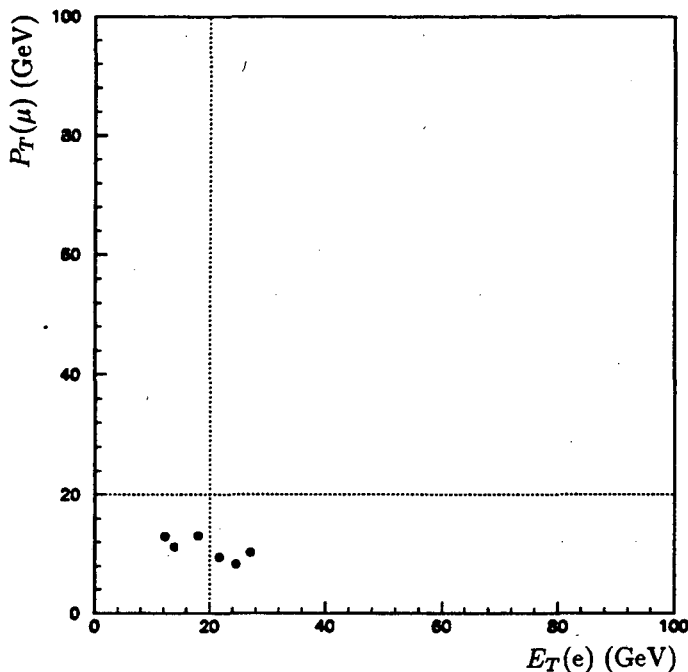


Figure 11: Muon P_T vs. electron E_T .

trigger on jets all the way down to $|\eta| = 3.2$. The preliminary inclusive jet cross section²² is shown in Fig. 12 for a data sample corresponding to 130 nb^{-1} of luminosity. The jets were reconstructed using a cone algorithm, with the cone radius = 0.7 (in $\eta - \phi$ space). The band in Fig. 12 is the upper and lower limit for the cross section including the current energy scale uncertainty. We have also measured the 2-jet double differential cross-sections²³ out to rapidities of 3.2 where the structure functions have considerable impact upon the results.

The full coverage of the DØ calorimeters to $|\eta| = 4.0$ and their fine segmentation and good energy resolution allow us to make a good measurement of direct photon production. Direct photons in the central region ($|\eta| < 0.9$) and in the P_T range of 14–90 GeV/c were searched for in the same 130 nb^{-1} sample of data used for the jet studies. The photons were required to have a transverse and longitudinal shape χ^2 which agrees with test beam expectations,¹⁹ to be isolated in a cone of $R = 0.4$ from the rest of the event, and to not have a track nearby. Backgrounds due to π^0 which pass the cuts were estimated through study of the ratio of 1-photon and 2-photon conversions in the tracking material, and by Monte Carlo simulations. Both methods are in agreement, finding that the fraction of photons in the candidate sample is 0.42 ± 0.14 . The resulting direct photon cross section²⁴ is shown in Fig. 13. The errors include an estimate of the systematic errors. It is seen that the data agree well with a next to leading order calculation.²⁵

The measurement of $W+Jet$ production is a good tool for testing QCD, as the

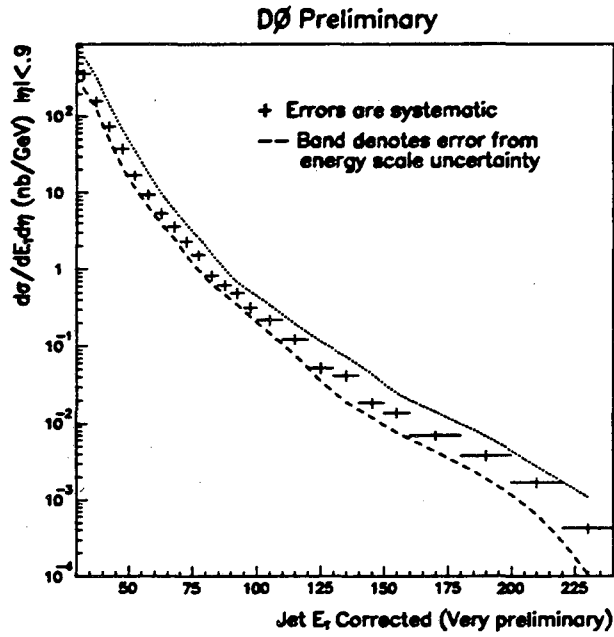


Figure 12: Inclusive jet cross section vs. jet E_T .

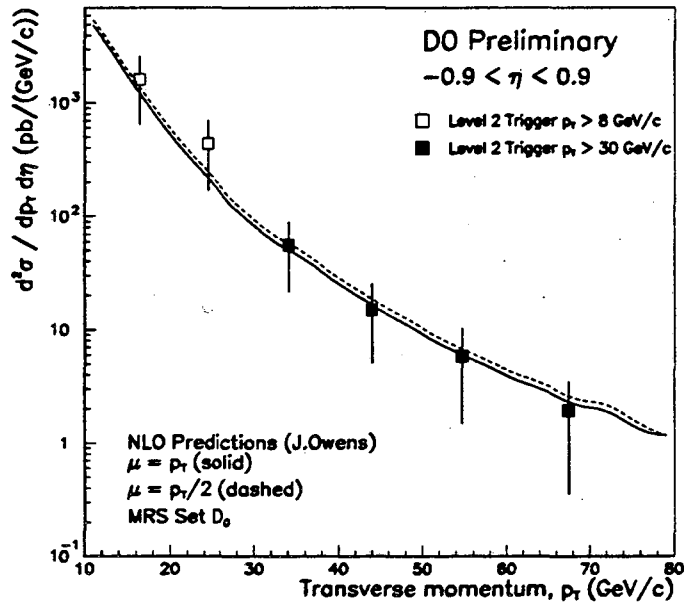


Figure 13: Direct photon cross section vs. photon P_T .

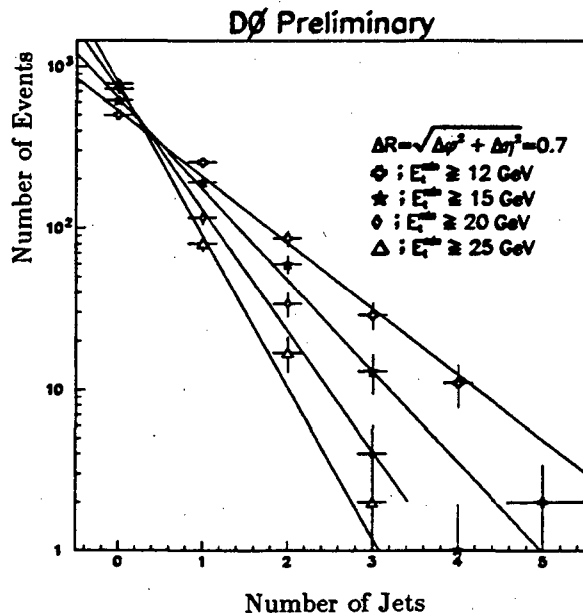


Figure 14: Jet multiplicity distribution for W events, for various values of the minimum E_T of the jets. The lines are logarithmic fits to the data.

next to leading order theoretical prediction for $W+0Jet$ and $W+1Jet$ is now available. In addition, one can use $W+Jet$ production to measure the strong coupling constant, α_s . The jet multiplicity distribution was studied²⁶ for the 882 $W \rightarrow e\nu$ event sample described above in the electroweak section. Figure 14 shows the number of events as a function of the number of jets associated with the W boson, for various values of the minimum E_T of the jets. It is seen that the distributions become steeper as the minimum jet E_T increases. This behavior will enable us to both test QCD and eventually measure α_s .

2.4 B Physics

The DØ detector has excellent muon coverage for the full solid angle ($|\eta| < 3.2$), and with the toroids we can measure the charge and momentum of the muons. Because of the muon system's compactness and large number of interaction lengths of material, the backgrounds from decay in flight and punchthrough are small. In addition, muons can be identified within jets. Inclusive single muon production has been measured,²⁷ and the P_T spectrum is shown in Fig. 15. These muons had hits in all three muon chamber layers, a track pointing back to the vertex, an appropriate energy deposit in the calorimeter, a central tracking chamber track match, and were not back-to-back with other tracks. Jets were found using a cone algorithm with a cone radius of 0.7 (in $\eta - \phi$ space), and at least one jet was required to be near the muon track. Also shown in Fig. 15 is the Monte Carlo expectation from b and c quarks, normalized to the total number of events. It is seen that the shapes agree well.

We have also observed dimuon production with jets,²⁸ and our measurement

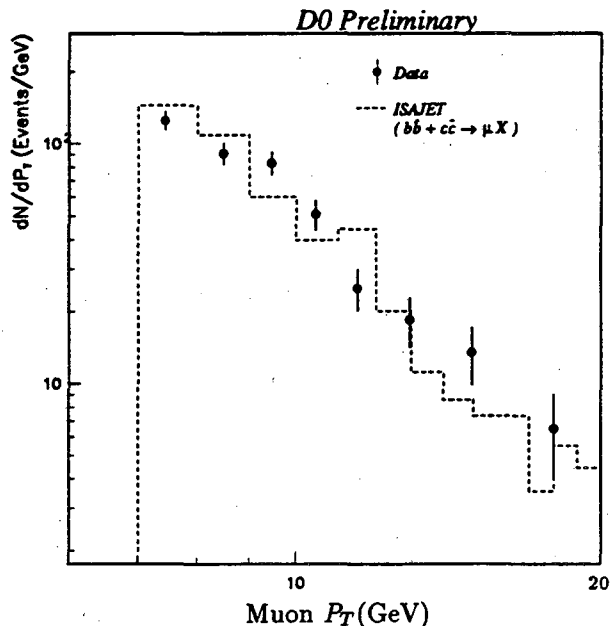


Figure 15: Inclusive muon P_T spectrum.

of the ratio of same sign events to opposite sign events is consistent with previous measurements of $B_0\bar{B}_0$ mixing.

Electrons can also be used to study b quark systems. In Fig. 16 we see a plot of the invariant mass of di-electrons, showing a clear $\Upsilon \rightarrow ee$ signal.

2.5 New Particle Searches

In the minimal supersymmetric extension of the Standard Model, gluinos and squarks either “decay directly” into the lightest neutralino (with large \cancel{E}_T and high E_T jets) or “cascade decay” through several supersymmetric particles and finally into the lightest neutralino (with less \cancel{E}_T , softer jets, and possible leptons). Thus the DØ detector’s excellent \cancel{E}_T resolution and acceptance for multijets and leptons will play an important role here. A search for squarks and gluinos was done,²⁹ involving purely hadronic decays, with a data sample corresponding to 140 nb^{-1} . We required three jets in the event (with each jet having $E_T > 20 \text{ GeV}$), $\cancel{E}_T > 30 \text{ GeV}$, and angular cuts on the jets and \cancel{E}_T to remove QCD backgrounds. No events were left after these cuts. These results clearly rule out squark and gluino masses both equal to $100 \text{ GeV}/c^2$, for which we would expect 6.9 ± 2.2 events after the above cuts.

Leptoquarks carry both color quantum numbers and lepton quantum numbers, and can decay, for example, into a lepton and a quark. In composite models, leptoquarks are the natural result of different combinations of the constituents of quarks and leptons. A search was done³⁰ for scalar leptoquarks, looking for events with 2 electrons and 2 jets, with a data sample corresponding to 0.8 pb^{-1} . Both

D0 preliminary

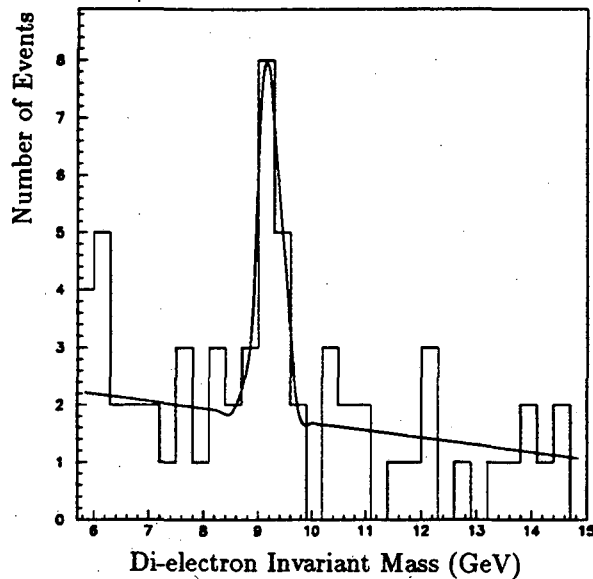


Figure 16: Di-electron invariant mass distribution.

electrons and jets were required to have $E_T > 20$ GeV. The electrons were required to be clean, isolated electrons. After removing one event that was consistent with $Z(\rightarrow ee) + 2jets$, no events were left after these cuts. Assuming a 100% branching ratio into the electron + quark decay mode, we have used this result to set a lower leptoquark limit of 74 GeV, at 95% CL.

3. Conclusion

The D0 Detector has been installed at the Fermilab Tevatron Collider, and is currently taking physics data. Preliminary physics results, based on the first three months of data taking after commissioning, have been presented in the areas of electroweak, QCD, B physics, top and new particle searches. We have rapidly begun to use D0 to do exciting physics.

4. Acknowledgements

I am indebted to the many D0 physicists who presented the latest D0 physics results at the DPF meeting and made their results available to me for this summary, and to all the members of the D0 Collaboration for their successful efforts in bringing the D0 Experiment to its productive physics phase. I would also like to thank Tony Spadafora for his help with the electronic integration of many of the figures used here, and Tony, Paul Grannis and David Buchholz for their critical reading of this paper. This work was supported by the U.S. Department of Energy

and the National Science Foundation.

5. References

1. Design report for the DØ Experiment at the Fermilab Antiproton-Proton Collider, Fermilab, November 1984 (unpublished).
2. P.D. Grannis, in the *Proceedings of Les Rencontres de Physique de la Vallée d'Aoste on Results and Perspectives in Particle Physics, La Thuile*, March 1987, edited by M. Greco (Editions Frontieres, 1987) p. 253.
3. C. Brown, *et al.*, *Nucl. Instr. and Meth.* A279 (1989) 331; J.M. Butler, *et al.*, *Nucl. Instr. and Meth.* A290 (1990) 122.
4. D. Green, *et al.*, *Nucl. Instr. and Meth.* A244 (1985) 356.
5. A.R. Clark *et al.*, *Nucl. Instr. and Meth.* A279 (1989) 243.
6. A.R. Clark *et al.*, *Nucl. Instr. and Meth.* A315 (1992) 193.
7. J.F. Detoeuf *et al.*, *Nucl. Instr. and Meth.* A265 (1988) 157.
8. T. Behnke, Ph.D. Thesis, SUNY, Stony Brook (1989); D. Pizzuto, Ph.D. Thesis, SUNY, Stony Brook (1991).
9. R.E. Avery *et al.*, DØ Note 1567, to be published in the *IEEE Trans. in Nucl. Sci.*
10. H. Aihara *et al.*, LBL-31378 (July 1992), to be published in *Nucl. Instr. and Meth.*
11. J. Christenson, to be published in the *Proceedings of the Third International Conference on Calorimetry in High Energy Physics, Corpus Christi, Texas*, September, 1992.
12. S. Abachi *et al.*, FNAL-PUB-92/162, to be published in *Nucl. Instr. and Meth.*
13. P. Bhat, "Low Energy Response of the DØ Calorimeter and Jet Energy Measurement", these Proceedings.
14. Jan Guida, DØ Note 1510, to be published in the *Proceedings of the Third International Conference on Calorimetry in High Energy Physics, Corpus Christi, Texas*, September, 1992.
15. M. Abolins *et al.*, *Nucl. Instr. and Meth.* A289 (1990) 543.
16. J. Linnemann, DØ Note 1519, to be published in the *Proceedings of the Conference on Computing in High Energy Physics, Annecy, France*, September, 1992; and also these Proceedings.
17. D. Wood, "W and Z Decays to Muons at DØ", these Proceedings.
18. N. Graf, "W and Z Decays to Electrons at DØ", these Proceedings.
19. M. Narain, "Electron Identification in the DØ Detector", these Proceedings.

20. R. Partridge, "Search for the Top Quark in Dilepton Events with $D\bar{O}$ ", these Proceedings.
21. B. Klima, "Search for the Top Quark in Electron+Jets Events in $D\bar{O}$ ", these Proceedings.
22. R. Astur, "Inclusive Jet Distributions at $D\bar{O}$ ", these Proceedings.
23. G. Blazey, "Dijet Differential Distributions", these Proceedings.
24. G. Snow, "Direct Photon Production at $D\bar{O}$ ", these Proceedings.
25. H. Baer, J. Ohnemus, J.F. Owens, *Phys. Lett. B* **234** (1990) 127, and private communication.
26. J. Yu, "W+Jet Production with $D\bar{O}$ ", these Proceedings.
27. K. Bazizi, "Inclusive Single Muon Production with $D\bar{O}$ ", these Proceedings.
28. S. Igarashi, "Dimuon Production at $D\bar{O}$ ", these Proceedings.
29. M. Paterno, "A Search for Squarks and Gluinos with $D\bar{O}$ ", these Proceedings.
30. W. Merritt, "Search for Scalar Leptoquarks in $D\bar{O}$ ", these Proceedings.

LAWRENCE BERKELEY LABORATORY
UNIVERSITY OF CALIFORNIA
TECHNICAL INFORMATION DEPARTMENT
BERKELEY, CALIFORNIA 94720